

Cite this: *RSC Adv.*, 2017, 7, 45742Received 29th July 2017
Accepted 19th September 2017

DOI: 10.1039/c7ra08381e

rsc.li/rsc-advances

Preparation of porous TiO₂ photocatalysts with different crystal phases and high catalytic activity by simple calcination of titanate nanofibers†

Yulan Peng,^{‡a} Xiaojun Shen,^{‡b} Lingzhi Wang,^{‡b} Baozhu Tian,^a Yongdi Liu,^c Haijun Chen,^d Juying Lei^{‡*c} and Jinlong Zhang^{‡*a}

A simple method has been developed to prepare porous TiO₂ photocatalysts with different crystal phases and large surface area by calcining titanate nanofibers under different temperatures. All the products exhibited excellent photocatalytic activity for RhB degradation under ultraviolet light irradiation.

Introduction

As a common inorganic semiconductor material, titanium dioxide (TiO₂) has become the most interesting, and in-depth studied semiconductor material because of its good photocatalytic activity, fine photoelectric effect, high photostability, low toxicity to humans and so on.^{1–3} However, its crystal composition and microstructure have a great influence on its photocatalytic activity. So far, intense studies have focused on how to efficiently control these affecting factors to achieve a coordinated effect to promote its photocatalytic performance. There are four main crystalline phases of TiO₂: anatase, rutile, brookite and TiO₂ (B). Among them, rutile with excellent stability is widely applied in paints⁴ and dye-sensitized solar cells.⁵ The anatase phase is preferred for applications in photocatalysis, due to its high potential conduction band edge energy.⁶ Thus, when designing TiO₂ as a photocatalyst, phase control must be deeply considered. At the same time, it is also expected that designing TiO₂ with a porous microstructure that provides more surface active sites will also result in promoting the photocatalytic performance.

Meanwhile, in recent years, a great number of studies have been done on titanate nanostructures,⁷ particularly, nanotubes,⁸ and nanowires,⁹ which have reported that one-

dimensional titanate nanostructures have potential applications in many ways, such as can be applied for photocatalysis,¹⁰ hydrogen storage,¹¹ lithium-ion battery,¹² and solar cells.¹³ What's more, several studies reported that titanate can be converted to TiO₂, under certain reaction conditions.^{14,15} Therefore, the research on titanate and TiO₂ nano-materials possesses both theoretical and practical significance. To date, several methods have been developed to transform titanate into nano-TiO₂ with different phases and morphology such as hydrothermal treatment with the assistance of urea¹⁶ and direct anodization of titanate in different electrolytes at room temperature.¹⁷ But the product is always not separated from each other in regular manner and the process is complicated and considered not environmentally friendly.

In this work, we developed a simple method to transform titanate nanofiber into different phase of porous nano-TiO₂. In details, the titanate nanofiber was firstly prepared through hydrothermal at 180 °C for 12 h in a low alkali concentration. After calcinated at different temperatures, the titanate nanofiber transformed into porous TiO₂ with different crystalline phases which were then applied in the photocatalytic degradation of RhB. The experimental results demonstrated that the catalysts with anatase phases and mesoporous microstructure have the best photocatalytic activities. Our work reveals that both crystalline phases and microstructure have great influence on the photocatalytic activity, and by controlling the annealing temperature we can get the best performance of the samples. Along with many advantages of the synthesis process, such as being surfactant-free and easy to operate, the synthesis method developed in this study provides a new inspiration for further investigation to the preparation of TiO₂ catalysts with advanced structures and high photocatalytic activity.

Results and discussion

The crystal structure and the average grain size of different samples were studied by X-ray diffraction (XRD). Fig. 1 shows

^aKey Lab for Advanced Materials and Institute of Fine Chemicals, School of Chemistry and Molecular Engineering, East China University of Science and Technology, 130 Meilong Road, Shanghai 200237, P. R. China. E-mail: jlzhang@ecust.edu.cn

^bState Environmental Protection Key Laboratory of Environmental Risk Assessment and Control on Chemical Process, East China University of Science and Technology, 130 Meilong Road, Shanghai 200237, P. R. China. E-mail: lejuying@ecust.edu.cn

^cFaculty of Chemistry & Material Engineering, Wenzhou University, 276 Xueyuan Road, Wenzhou 325027, Zhejiang Province, P. R. China

^dDepartment of Electronics and Tianjin Key Laboratory of Photo-Electronic Thin Film Device and Technology, Nankai University, Tianjin, 300071, China

† Electronic supplementary information (ESI) available. See DOI: 10.1039/c7ra08381e

‡ These authors contributed equally to this work.

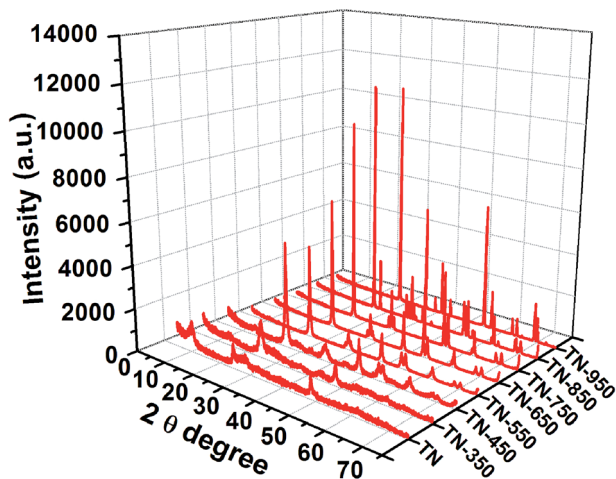


Fig. 1 XRD patterns of the titanate nanofiber and its calcined products at different temperatures.

the XRD patterns of the samples before and after 2 h of calcination of the titanate nanofibers at different temperatures. It can be found that after calcining at 350 °C for 2 h, the titanate nanofibers were transformed into $\text{TiO}_2\text{-B}$ phase, which is a metastable status of TiO_2 .¹⁸ With increasing the temperature to 450 °C, the sample become mainly anatase TiO_2 with a small amount of $\text{TiO}_2\text{-B}$ phase. In the XRD patterns of products calcined from 550 °C to 750 °C, each diffraction peak coincides with that of anatase TiO_2 ,^{19,20} obviously indicating the products were pure anatase TiO_2 . When the calcination temperature was increased from 450 °C to 750 °C, the peak intensity of anatase in the XRD spectra for the products increased significantly, indicating that the degree of crystallinity of anatase increases with the increase of the calcination temperature. Meanwhile, the width of the anatase (101) diffraction peak becomes narrower and narrower, suggesting that the TiO_2 grain grows and becomes larger in size. When the temperature reached 850 °C, there were both diffraction peaks of rutile and anatase, clearly demonstrating that the transition temperature of anatase to rutile was about 850 °C. As the calcination temperature up to 950 °C, the product transformed to pure rutile, which demonstrated that there is a narrow temperature range from anatase to rutile. A lot of researches reported the occurrence of the phase transition temperature and the temperature range of phase transition depend on the particle size, morphology of crystals, and other additives.²¹ Particularly, in this experiment, phase transition temperature from anatase to rutile has a narrow range (about 850–950 °C), which may be due to the formation of TiO_2 was dehydrated by titanate-H. Therefore, it can be concluded that with the increase of the calcination temperature, the products experienced phase changing process as “Titanate \rightarrow $\text{TiO}_2\text{-B}$ \rightarrow $\text{TiO}_2\text{-B}$ + Anatase \rightarrow Anatase \rightarrow Anatase + Rutile \rightarrow Rutile”.

The average particle sizes of TiO_2 in the calcined products were obtained by the formula of Scherrer, referring to Table S1.† During the increase of calcination temperature from 450 °C to 750 °C, the average grain size of anatase particles increases from

12.9 nm to 31.6 nm. When the temperature reached 850 °C, rutile occurred, which also resulted in a significant increase in grain size. If the calcination temperature exceeded 850 °C, the rutile grains reached 105 nm, due to the transformation of anatase to rutile with the sintering and growth of rutile.

The surface area and pore-size distribution of the samples were investigated by N_2 adsorption–desorption measurements (Fig. 2). According to BDDT (Brunauer–Deming–Deming–Teller) classification criteria, the isotherms of the samples are typical IV curves, and H3 hysteresis loops can be observed for the samples under different calcination temperature; these are typical isotherms of mesoporous materials.^{22–24} With the increasing of calcination temperature, adsorption–desorption isotherm hysteresis loop of the products shifts to the area with relatively higher pressure, and the area of hysteresis loop is gradually reduced. When the calcination temperature is higher than 750 °C, the hysteresis loop almost disappeared, indicating that mesoporous structure was destroyed at a higher temperature. The specific surface area, pore volume and pore size of different products were calculated which is presented in Table S2.† It can be seen that with the calcination temperature increases, the surface area and pore volume decrease. When the titanate nanofibers were calcined at 750 °C, the BET surface area and pore volume both decreased respectively to $21.0 \text{ m}^2 \text{ g}^{-1}$ and $0.098 \text{ cm}^3 \text{ g}^{-1}$, which was because the collapse of the pore structure and the growth of TiO_2 grains. With further increase of the calcination temperature, the growth of rutile TiO_2 grains led to larger pores between grains and the BET surface area, pore volume and pore size further decreased. The BET surface area of TN-850 was only $3.8 \text{ m}^2 \text{ g}^{-1}$ and its corresponding pore volume was only $0.006 \text{ cm}^3 \text{ g}^{-1}$. For pure rutile TiO_2 , the BET surface area is only $1.2 \text{ m}^2 \text{ g}^{-1}$ and the pore volume is only $0.006 \text{ cm}^3 \text{ g}^{-1}$.

The morphology of different samples are got from SEM images (Fig. 3). Fig. 3A presents the titanate nanofiber before calcination treatment, in which it can be found that the precursor nanofibers are intertwined structure. After calcined under different temperatures, the end of the nanofibers were sintered (Fig. 3B–E), so the morphology has little differences in different temperatures, even though they all derived from the

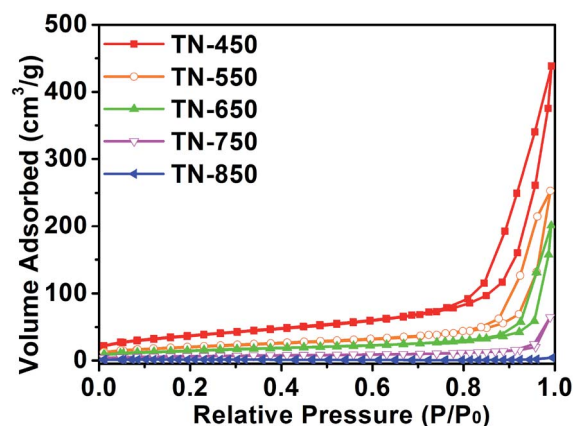


Fig. 2 N_2 adsorption–desorption isotherms of different samples.



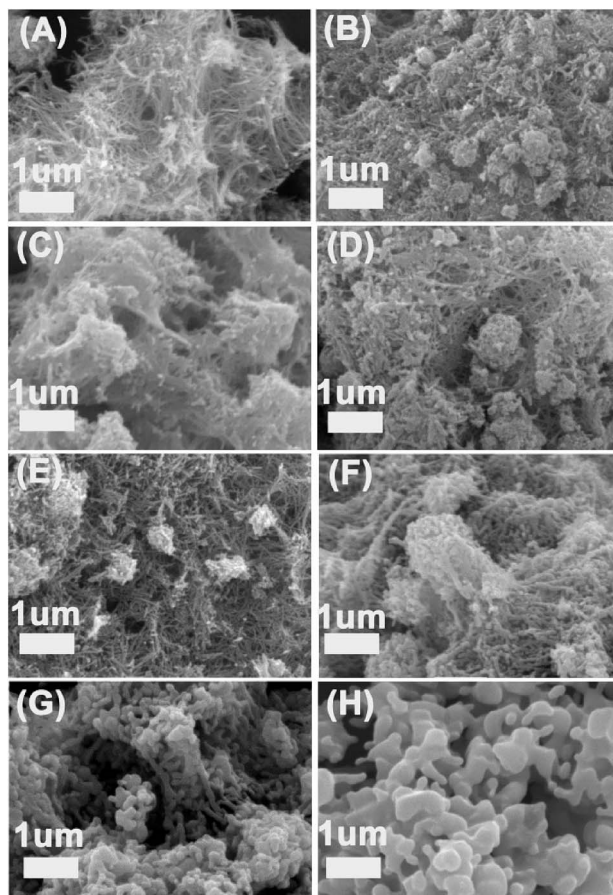


Fig. 3 SEM images of the titanate nanofiber and its calcined products: (A) TN, (B) TN-350, (C) TN-450, (D) TN-550, (E) TN-650, (F) TN-750, (G) TN-850, (H) TN-950.

porous nanofibers' accumulation. If the calcination temperature further increased, we found that the structures of the nanofibers were heavily destroyed. When the calcination temperatures were up to 850 °C and 950 °C, along with the process of phase conversion, the structure of the nanofibers were completely destroyed. In addition, the size of TiO₂ particles increased significantly as shown in Fig. 3G and H, which is consistent with the XRD and BET datas.

The photoactivity of different samples are test through photodegrade RhB under UV-light. As we can see from the Fig. 4, whether in a low concentration (10 mg L⁻¹) or a higher concentration (20 mg L⁻¹) of RhB solution, the sample which calcined at 650 °C performed best. Proved by the XRD figure, the phase of TiO₂ is pure anatase, and anatase is regarded as the more active phase for photocatalysis due to its surface chemistry and potentially high conduction band edge energy.⁵ Although samples calcinatd from 550–750 °C all exhibits pure anatase phase, but the TN-650 has retained the mesoporous structure and has the biggest pore size among those samples, which may be the reason why the sample has the best performance for degradation RhB. In the degradation of 10 mg L⁻¹ of RhB aqueous solution, almost all the RhB was removed in 50 minutes, while in the degradation of 20 mg L⁻¹ of RhB, the time was 80 minutes, which was both better than the

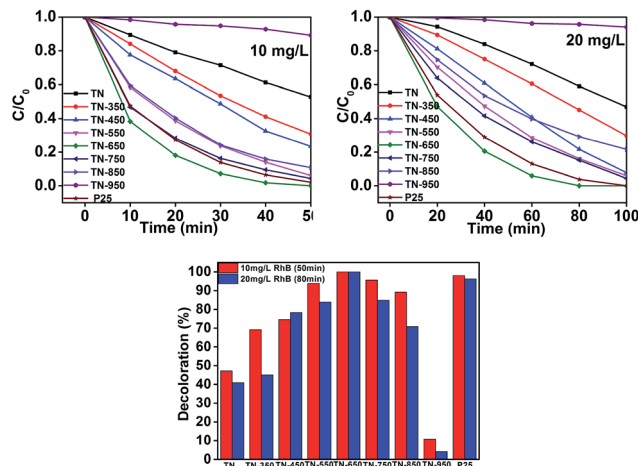


Fig. 4 Photocatalytic degradation of 10 mg L⁻¹ and 20 mg L⁻¹ RhB aqueous solution with different catalysts.

photocatalytic activity of P25. Fig. 4 also shows after calcination at 350–850 °C, the photocatalytic activity was significantly increased compared with the titanate nanofiber. This can be attributed to that TiO₂ with good crystallinity (according to XRD figures) could be obtain after the calcination treatments. With the increasing the temperature between 350–650 °C, the photocatalytic activity of the product increases, despite BET specific surface and pore volume of samples decreases, increasing anatase crystallinity of products much more better increases the performance of photocatalyst. When the calcination temperature was higher than 650 °C, the BET surface area and pore volume of the products had significant decrease, which is the main reason for the decreased photocatalytic activity. As the temperature further increasing, phase of rutile arose. The sample TN-850 has a BET surface area of only 3.8 m² g⁻¹ and a pore volume of only 0.006 cm³ g⁻¹, but its photocatalytic activity was significantly higher than that of TN-350, which can be attributed to its mixture phase of anatase and rutile. It was previously reported^{25–28} that mixed phase structure of TiO₂ can effectively improve the photocatalytic activity. Obviously, the photocatalytic activity of the product TN-950 behaved extremely bad, due to TN-950 is pure rutile TiO₂, and the BET surface and pore volume are extremely low. Collectively, the photocatalytic activity is intimately related to the degree of crystallinity, the phase composition and its microstructure.

Conclusions

In summary, by simply calcining titanate nanofibers at different temperatures, porous TiO₂ photocatalysts with different crystal phases and photocatalytic activity were successfully obtained. With the increase of the calcination temperature, the product experiences phase changing process of “Titanate → TiO₂-B → TiO₂-B + Anatase → Anatase → Anatase + Rutile → Rutile”. The photocatalytic activity of the samples showed a first increasing and then decreasing trend, in which TN-650 prepared by calcination of the titante nanofibers at 650 °C showed the best



photocatalytic degradation activity, even higher than the commercial P25, due to its mesoporous microstructure and well crystalline phase of anatase. Furthermore, it is entirely possible that this preparation method can be used to get other photocatalysts which can withstand high temperature.

Conflicts of interest

There are no conflicts to declare.

Acknowledgements

This work was financially supported by National Nature Science Foundation of China (21407049, 21377038, 21237003, 21677048), Science and Technology Commission of Shanghai Municipality (16JC1401400, 17520711500), China Postdoctoral Science Foundation (2015T80409).

Notes and references

- 1 J. Zhang, Y. Wu, M. Xing, S. A. K. Leghari and S. Sajjad, *Energy Environ. Sci.*, 2010, **3**, 715–726.
- 2 L. Hu, Y. Zhang, S. Zhang and B. Li, *RSC Adv.*, 2016, **6**, 43098–43103.
- 3 W. Wang, Y. Liu, J. Qu, Y. Chen and Z. Shao, *RSC Adv.*, 2016, **6**, 40923–40931.
- 4 R. Verma and S. Samdarshi, *J. Alloys Compd.*, 2015, **629**, 105–112.
- 5 N.-G. Park, J. Van de Lagemaat and A. Frank, *J. Phys. Chem. B*, 2000, **104**, 8989–8994.
- 6 O.-O. Prieto-Mahaney, N. Murakami, R. Abe and B. Ohtani, *Chem. Lett.*, 2009, **38**, 238–239.
- 7 Y. Zhang, Z. Jiang, J. Huang, L. Y. Lim, W. Li, J. Deng, D. Gong, Y. Tang, Y. Lai and Z. Chen, *RSC Adv.*, 2015, **5**, 79479–79510.
- 8 Y. Tang, Z. Jiang, Q. Tay, J. Deng, Y. Lai, D. Gong, Z. Dong and Z. Chen, *RSC Adv.*, 2012, **2**, 9406–9414.
- 9 M. H. A. Rehim, A. M. Youssef, H. Al-Said, G. Turkey and M. Aboaly, *RSC Adv.*, 2016, **6**, 94556–94563.
- 10 D. K. Chacko, A. A. Madhavan, T. A. Arun, *et al.*, *RSC Adv.*, 2013, **3**, 24858–24862.
- 11 Z. Weng, H. Guo, X. Liu, *et al.*, *RSC Adv.*, 2013, **3**, 24758–24775.
- 12 Q. Wang, Z. Wen and J. Li, *Inorg. Chem.*, 2006, **45**, 6944–6949.
- 13 J. Qiu, Y. Qiu, K. Yan, *et al.*, *Nanoscale*, 2013, **5**, 3245–3248.
- 14 X. Shen, J. Zhang and B. Tian, *J. Mater. Sci.*, 2012, **47**, 3855–3866.
- 15 H. Li, X. Shen, Y. Liu, L. Wang, J. Lei and J. Zhang, *J. Alloys Compd.*, 2016, **687**, 927–936.
- 16 K. Kobayakawa, Y. Murakami and Y. Sato, *J. Photochem. Photobiol., A*, 2005, **170**, 177–179.
- 17 D. Gong, C. A. Grimes, O. K. Varghese, W. Hu, R. Singh, Z. Chen and E. C. Dickey, *J. Mater. Res.*, 2001, **16**, 3331–3334.
- 18 B. Zhao, F. Chen, W. Qu and J. Zhang, *J. Solid State Chem.*, 2009, **182**, 2225–2230.
- 19 A. A. Ashkarran, M. Ghavamipour, H. Hamidinezhad and H. Haddadi, *Res. Chem. Intermed.*, 2015, **41**, 7299–7311.
- 20 H. Li, L. Zhou, L. Wang, Y. Liu, J. Lei and J. Zhang, *Phys. Chem. Chem. Phys.*, 2015, **17**, 17406–17412.
- 21 Q. Sheng, S. Yuan, J. Zhang and F. Chen, *Microporous Mesoporous Mater.*, 2006, **87**, 177–184.
- 22 M. Pudukudy, Z. Yaakob and R. Rajendran, *Mater. Lett.*, 2014, **136**, 85–89.
- 23 C. Cheng, D. Lu, B. Shen, Y. Liu, J. Lei, L. Wang, J. Zhang and M. Matsuoka, *Microporous Mesoporous Mater.*, 2016, **226**, 79–87.
- 24 J. Lei, L. Yang, D. Lu, X. Yan, C. Cheng, Y. Liu, L. Wang and J. Zhang, *Adv. Opt. Mater.*, 2015, **3**, 57–63.
- 25 J. Zhu, J. Zhang, F. Chen and M. Anpo, *Mater. Lett.*, 2005, **59**, 3378–3381.
- 26 H. Li, X. Shen, Y. Liu, L. Wang, J. Lei and J. Zhang, *J. Alloys Compd.*, 2015, **646**, 380–386.
- 27 M. Morozova, P. Dytrych, L. Spacilova and O. Solcova, *Res. Chem. Intermed.*, 2015, **41**, 9307–9318.
- 28 J. Lei, H. Li, J. Zhang and M. Anpo, in *Low-Dimensional and Nanostructured Materials and Devices*, Springer, 2016, pp. 423–460.

